

Luminescent Solar Concentrators – A review of recent results

Wilfried G.J.H.M. van Sark,^{1,*} Keith W.J. Barnham,² Lenneke H. Slooff,³
Amanda J. Chatten,² Andreas Büchtemann,⁴ Andreas Meyer,⁵ Sarah J. McCormack,⁶
Rolf Koole,⁷ Daniel J. Farrell,² Rahul Bose,² Evert E. Bende,³ Antonius R. Burgers,³
Tristram Budel,³ Jana Quilitz,⁴ Manus Kennedy,⁶ Toby Meyer,⁵ C. De Mello Donegá,⁷
Andries Meijerink,⁷ Daniel Vanmaekelbergh⁷

¹Science, Technology and Society, Copernicus Institute of Sustainable Development and Innovation,
Utrecht University, Heidelberglaan 2, 3584 CS Utrecht, the Netherlands

²Department of Physics, Imperial College London, South Kensington Campus, London SW7 2AZ, United Kingdom

³ECN Solar Energy, P.O. Box 1, 1755 ZG Petten, the Netherlands

⁴Fraunhofer Institute for Applied Polymer Research (IAP), Geiselbergstraße 69, 14476 Potsdam, Germany

⁵Solaronix SA, Rue de l'Ouriette 129, 1170 Aubonne, Switzerland

⁶Focas Institute, School of Physics, Dublin Institute of Technology, Kevin St, Dublin 8, Ireland

⁷Chemistry of Condensed Matter, Debye Institute for Nanomaterials Science, Utrecht University,
Princetonplein 1, 3584 CC Utrecht, the Netherlands

*Corresponding author: w.g.j.h.m.vansark@uu.nl

Abstract: Luminescent solar concentrators (LSCs) generally consist of transparent polymer sheets doped with luminescent species. Incident sunlight is absorbed by the luminescent species and emitted with high quantum efficiency, such that emitted light is trapped in the sheet and travels to the edges where it can be collected by solar cells. LSCs offer potentially lower cost per Wp. This paper reviews results mainly obtained within the framework of the Fullspectrum project. Two modeling approaches are presented, i.e., a thermodynamic and a ray-trace one, as well as experimental results, with a focus on LSC stability.

©2008 Optical Society of America

OCIS codes: (130.7405) Wavelength conversion devices; (040.5350) Photovoltaic; (130.0250) Optoelectronics

References and links

1. W. G. J. H. M. Van Sark, G. W. Brandsen, M. Fleuster, and M. P. Hekkert, "Analysis of the silicon market: Will thin films profit?," *Energy Pol.* **35**, 3121 (2007).
2. M. A. Green, *Third Generation Photovoltaics, Advanced Solar Energy Conversion* (Springer Verlag, Berlin, Germany, 2003).
3. A. Martí and A. Luque, eds. "Next Generation Photovoltaics, High Efficiency through Full Spectrum Utilization," in *Series in Optics and Optoelectronics*, R.G.W. Brown and E.R. Pike. eds. (Institute of Physics Publishing: Bristol, UK, 2004).
4. A. Luque and A. Martí, "Increasing the Efficiency of Ideal Solar Cells by Photon Induced Transitions at Intermediate Levels," *Phys. Rev. Lett.* **78**, 5014-5017 (1997).
5. K. Barnham, J. L. Marques, J. Hassard, and P. O'Brien, "Quantum-dot concentrator and thermodynamic model for the global redshift," *Appl. Phys. Lett.* **76**, 1197-1199 (2000).
6. T. Trupke, M. A. Green, and P. Würfel, "Improving solar cell efficiencies by down-conversion of high-energy photons," *J. Appl. Phys.* **92**, 1668-1674 (2002).
7. T. Trupke, M. A. Green, and P. Würfel, "Improving solar cell efficiencies by up-conversion of sub-band-gap light," *J. Appl. Phys.* **92**, 4117-4122 (2002).
8. A. Goetzberger and W. Greubel, "Solar Energy Conversion with Fluorescent Collectors," *Appl. Phys.* **14**, 123-139 (1977).
9. V. Wittwer, W. Stahl, and A. Goetzberger, "Fluorescent planar concentrators," *Sol. Energy Mater.* **11**, 187-197 (1984).
10. A. Luque, A. Martí, A. Bett, V. M. Andreev, C. Jaussaud, J. A. M. van Roosmalen, J. Alonso, A. Räuber, G. Strobl, W. Stolz, C. Algora, B. Bitnar, A. Gombert, C. Stanley, P. Wahnnon, J. C. Conesa, W. G. J. H. M. Van Sark, A. Meijerink, G. P. M. Van Klink, K. Barnham, R. Danz, T. Meyer, I. Luque-Heredia, R. Kenny, C. Christofides, G. Sala, and P. Benítez, "FULLSPECTRUM: a new PV wave making more efficient use of the solar spectrum," *Sol. Energy Mater. Sol. Cells* **87**, 467-479 (2005).

11. X. Peng, M. C. Schlamp, A. V. Kadavanich, and A. P. Alivisatos, "Epitaxial Growth of Highly Luminescent CdSe/CdS Core/Shell Nanocrystals with Photostability and Electronic Accessibility," *J. Am. Chem. Soc.* **119** 7019-7029 (1997)
12. A. J. Chatten, D. J. Farrell, C. M. Jermyn, P. A. Thomas, B. F. Buxton, A. Büchtemann, R. Danz, and K. W. J. Barnham, "Thermodynamic Modelling of the Luminescent Solar Concentrator," in *Proceedings of 31st IEEE Photovoltaic Specialists Conference* (IEEE, New York, USA, 2005) pp. 82-85.
13. A. J. Chatten, K. W. J. Barnham, B. F. Buxton, N. J. Ekins-Daukes, and M. A. Malik, "Quantum Dot Solar Concentrators," *Semiconductors* **38**, 609-617. (2004).
14. A. A. Earp, G. B. Smith, P. D. Swift, and J. Franklin, "Maximising the light output of a Luminescent Solar Concentrator," *Sol. Energy* **76**, 655-667 (2004).
15. T. Markvart, D. L., P. Kittidachachan, and R. Greef, "Detailed balance efficiency of ideal single-stage fluorescent collectors," in *Proceedings of Twentieth European Photovoltaic Solar Energy Conference*, W. Hoffmann, J.-L. Bal, H. Ossenbrink, W. Palz, and P. Helm, Eds. (WIP, Munich, Germany, 2005) pp. 171-174.
16. M. Carrascosa, S. Unamuno, and F. Agullo-Lopez, "Monte Carlo simulation of the performance of PMMA luminescent solar collectors," *Appl. Opt.* **22**, 3236-3241 (1983).
17. S. J. Gallagher, P. C. Eames, and B. Norton, "Quantum dot solar concentrator behaviour predicted using a ray trace approach," *J. Ambient Energy* **25**, 47-56 (2004).
18. U. Rau, F. Einsele, and G. C. Glaeser, "Efficiency limits of photovoltaic fluorescent collectors," *Appl. Phys. Lett.* **87**, 171101 (2003).
19. A. J. Chatten, K. W. J. Barnham, B. F. Buxton, N. J. Ekins-Daukes, and M. A. Malik, "The Quantum Dot Concentrator: Theory and Results," in *Proceedings of Third World Congress on Photovoltaic Energy Conversion (WPEC-3)*, K. Kurokawa, L. Kazmerski, B. McNelis, M. Yamaguchi, C. Wronski, and W. C. Sinke, Eds. (WPEC-3, Osaka, Japan, 2003) pp. 2657-2660.
20. A. J. Chatten, K. W. J. Barnham, B. F. Buxton, N. J. Ekins-Daukes, and M. A. Malik, "Quantum Dot Solar Concentrators and Modules," in *Proceedings of 19th European Photovoltaic Solar Energy Conference*, W. Hoffmann, J.-L. Bal, H. Ossenbrink, W. Palz, and P. Helm, Eds. (WIP, Munich, Germany; ETA, Florence, Italy, 2004), pp. 109-112.
21. E. A. Milne, "Radiative Equilibrium in Outer Layers of a Star," *Monthly Notices Roy. Astron. Soc. London* **81**, 361-388. (1921)
22. S. Chandrasekhar, *Radiative Transfer* (Clarendon, Oxford, UK, 1950).
23. A. J. Chatten, D. J. Farrell, B. F. Buxton, A. Büchtemann, and K. W. J. Barnham, "Thermodynamic Modelling of Luminescent Solar Concentrators and Modules," in *Proceedings of Twentyfirst European Photovoltaic Solar Energy Conference*, J. Poortmans, H. Ossenbrink, E. Dunlop, and P. Helm, Eds. (WIP, Munich, Germany, 2006), pp. 315-319.
24. A. J. Chatten, D. J. Farrell, R. Bose, M. G. Debije, A. Büchtemann, and K. W. J. Barnham, "Thermodynamic Modelling of Luminescent Solar Concentrators With Reduced Top Surface Losses," in *Proceedings of Twenty Second European Photovoltaic Solar Energy Conference*, G. Willeke, H. Ossenbrink, and P. Helm, Eds. (WIP, Munich, Germany, 2007), pp. 349-353.
25. M. G. Debije, R. H. L. Van der Blom, D. J. Broer, and C. W. Bastiaansen, "Using selectively-reflecting organic mirrors to improve light output from a luminescent solar concentrator," in *Proceedings of World Renewable Energy Congress IX* (2006).
26. A. R. Burgers, L. H. Slooff, R. Kinderman, and J. A. M. van Roosmalen, "Modeling of luminescent concentrators by ray-tracing," in *Proceedings of Twentieth European Photovoltaic Solar Energy Conference*, W. Hoffmann, J.-L. Bal, H. Ossenbrink, W. Palz, and P. Helm, Eds. (WIP, Munich, Germany, 2005) pp. 394-397.
27. L. H. Slooff, R. Kinderman, A. R. Burgers, A. Büchtemann, R. Danz, T. B. Meyer, A. J. Chatten, D. Farrell, K. W. J. Barnham, and J. A. M. Van Roosmalen, "The luminescent concentrator illuminated," *Proc. SPIE* **6197**, 1-8 (2006).
28. P. Polishuk, "Plastic Optical Fibers Branch Out," *IEEE Commun. Mag.* **140** (September 2006).
29. A. Zastrow, "Physikalische Analyse der Energieverlustmechanismen im Fluoreszenzkollektor," Ph.D. Thesis, Freiburg, 1981.
30. B. Richards and K. R. McIntosh, "Ray-tracing simulations of luminescent solar concentrators containing multiple luminescent species," in *Proceedings of Twentyfirst European Photovoltaic Solar Energy Conference*, J. Poortmans, H. Ossenbrink, E. Dunlop, and P. Helm, Eds., (WIP, Munich, Germany, 2006) pp. 185-188.
31. A. R. Burgers, L. H. Slooff, and M. G. Debije, "Reduction of escape cone losses in luminescent concentrators with cholesteric mirrors," *Technical digest PVSEC-17* (PVSEC-17, Fukuoka, Japan, 2007).
32. B. S. Richards, A. Shalav, and R. P. Corkish, "A low escape-con-loss luminescent solar concentrator," in *Proceedings of 19th European Photovoltaic Solar Energy Conference*, W. Hoffmann, J.-L. Bal, H. Ossenbrink, W. Palz, and P. Helm, Eds., (WIP, Munich, Germany, 2004), pp. 113-116.
33. M. Peters, J. C. Goldschmidt, P. Loeper, A. Gombert, and G. Willeke, "Application of photonic structures on fluorescent concentrators," in *Proceedings of Twenty Second European Photovoltaic Solar Energy Conference*, G. Willeke, H. Ossenbrink, and P. Helm, Eds. (WIP, Munich, Germany, 2007), pp. 177-181.

34. M. G. Debije, D. J. Broer, and C. W. M. Bastiaansen, "Effect of dye alignment on the output of a luminescent solar concentrator," in *Proceedings of Twenty Second European Photovoltaic Solar Energy Conferenc.*, G. Willeke, H. Ossenbrink, and P. Helm, Eds. (WIP, Munich, Germany, 2007), pp. 87-89.
35. M. Kennedy, S. J. McCormack, J. Doran, and B. Norton, "Modelling the effect of device geometry on concentration ratios of quantum dot solar concentrators," in *Proceedings of ISES World Solar Congress* (Beijing, China, 2007).
36. <http://www.basf.de>.
37. <http://www.cup.uni-muenchen.de/oc/langhals/S-13/>.
38. R. Koole, M. Van Schooneveld, J. Hilhorst, C. De Mello Donegá, D. C. 't Hart, A. Van Blaaderen, D. Vanmaekelbergh, and A. Meijerink, "On the Incorporation Mechanism of Hydrophobic Quantum Dots in Silica Spheres by a Reverse Microemulsion Method," *Chem. Mater.* **20**, 2503–2512 (2008).
39. R. Xie, U. Kolb, J. Li, T. Basche, and A. Mews, "Synthesis and Characterization of Highly Luminescent CdSe-Core CdS/Zn0.5Cd0.5S/ZnS Multishell Nanocrystals," *J. Am. Chem. Soc.* **127**, 7480-7488 (2005)
40. L. Carbone, C. Nobile, M. De Giorgi, F. D. Sala, G. Morello, P. Pompa, M. Hytch, E. Snoeck, A. Fiore, I. R. Franchini, M. Nadasan, A. F. Silvestre, L. Chiodo, S. Kudera, R. Cingolani, R. Krahn, and L. Manna, "Synthesis and Micrometer-Scale Assembly of Colloidal CdSe/CdS Nanorods Prepared by a Seeded Growth Approach," *Nano. Lett.* **7**, 2942-2950 (2007).
41. R. Kinderman, L. H. Slooff, A. R. Burgers, N. J. Bakker, A. Büchtemann, R. Danz, and J. A. M. van Roosmalen, "I-V Performance and Stability of Dyes for Luminescent Plate Concentrators," *J. Solar Energy Engin.* **129**, 277-282 (2007).
42. G. Seybold and G. Wagenblast, "New perylene and violanthrone dyestuffs for fluorescent collectors," *Dyes Pigm.* **11**, 303-317 (1989).
43. W. Stahl and A. Zastrow, "Fluoreszenzkollektoren," *Physik in unserer Zeit* **16**, 167(1985).

1. Introduction

Attaining higher conversion efficiencies at lower costs is the key driver in photovoltaics (PV) research and development and has been so for many decades. Today, the prices of PV modules are too high and widespread deployment of PV technology still needs financial support schemes, such as investment subsidies or feed-in tariffs, the latter being also a quality assurance check. Nevertheless, over the past 10 years the PV industry is experiencing average annual growth rates of 40% [1]. To reach lower cost per installed capacity (€/W), several routes are being pursued, all more or less directed towards a better use of the complete solar spectrum, and they are being referred to as Next or Third Generation PV [2,3]. Examples are intermediate band-gap cells [4], quantum dot concentrators [5] and down- and up-converters [6,7]. Conversion of the incident solar spectrum to monochromatic light would greatly increase the efficiency of solar cells. Down conversion was suggested in the late 1970s to be used in so-called luminescent solar concentrators (LSC), also referred to as fluorescent concentrators. To these LSCs solar cell(s) were attached [8]. LSCs consist of a highly transparent plastic, in which luminescent species, originally organic dye molecules, are dispersed, see Fig. 1. These dyes absorb incident light and isotropically emit it at a red-shifted wavelength, with high quantum efficiency. Internal reflection ensures collection of part of the emitted light in the solar cells at the side(s) of the plastic body. The energy of the emitted photons ideally is only somewhat larger than the band gap of the attached solar cells, to ensure near-unity conversion efficiency.

LSCs were developed as an alternative approach to lower the costs of PV. As both direct and diffuse light is concentrated by a factor of 5-10, without the need for expensive tracking, smaller silicon (or other) solar cells can be used. As the cost of the transparent plastic is expected to be (much) lower than the area cost of the solar cell the cost per Watt-peak is lower compared to the cost of a planar silicon solar cell. Also, LSCs are of special interest for building integrated PV applications.

The development of the LSC was initially limited by the performance of the luminescent dyes available some decades ago. Nevertheless, efficiencies of up to 4% have been reported for a stack of two plates ($40 \times 40 \times 0.3 \text{ cm}^3$), one being coupled to a GaAs solar cell, and the other to a Si solar cell [9]. Particular problems were the poor stability of the dyes under solar irradiation and the large re-absorption losses owing to significant overlap of the absorption and emission. Within the Fullspectrum project [10] the performance of both quantum dots

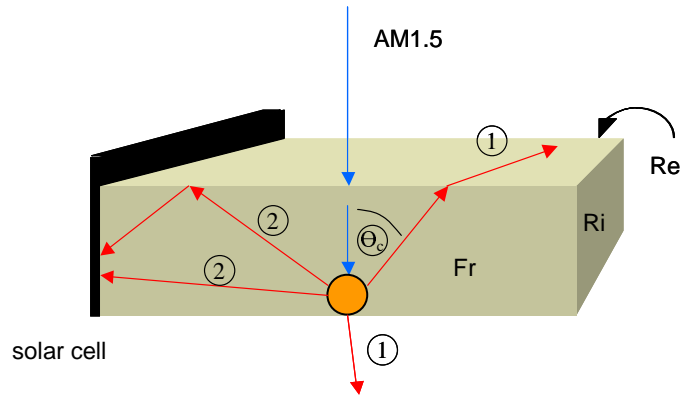


Fig. 1. Schematic 3D view of a luminescent concentrator. AM1.5 light is incident from the top. The light is absorbed by a luminescent particle. The luminescence from the particle is randomly emitted. Part of the emission falls within the escape cone (determined by the angle (θ_e)) and is lost from the luminescent concentrator at the surfaces (1). The other part of the luminescence is guided to the solar cell by total internal reflection (2).

(QDs) and organic dyes are being evaluated as the luminescent species in the LSC. The important characteristics of organic dyes are that they: (i) can provide extremely high luminescence quantum efficiency (LQE) (near unity), (ii) are available in a wide range of colours and, (iii) new molecular species are now available with better re-absorption properties that may also provide the necessary UV stability. QDs have advantages over dyes in that: (i) their absorption spectra are far broader, extending into the UV, (ii), their absorption properties may be tuned simply by the choice of nanocrystal size, and (iii) they are inherently more stable than organic dyes. Moreover, (iv) there is a further advantage in that the red-shift between absorption and luminescence is *quantitatively* related to the *spread* of QD sizes, which may be determined during the growth process, providing an additional strategy for minimising losses due to re-absorption [5]. However, as yet QDs can only provide reasonable LQE: a LQE > 0.8 has been reported for core-shell QDs [11].

This paper reviews recent results in LSC development, mainly obtained within the framework of the Fullspectrum project [10]. These encompass modeling and experimental work, as well as stability issues.

2. Modeling

Several groups have reported on the modeling of the LSC [12-18] Principally two different approaches are used, a detailed balance model which is based on the radiative energy transfer between mesh points in the concentrator plate, and a ray-tracing model in which every incoming photon is tracked and its fate determined. In the following these two approaches are detailed.

2.1 Thermodynamic modeling

Self-consistent 3D thermodynamic models for planar LSCs [13,19], modules [20] and stacks [12] have been developed which show excellent agreement with experiments on test devices. Detailed balance arguments relate the absorbed light to the emission using 3D fluxes and the thermodynamic models were derived by performing a Schwartzchild-Milne [21] type sampling of Chandrasekhar's radiative transfer equation [22], integrating the resulting differential equations over the volume of the concentrator and applying appropriate reflection boundary conditions. The resulting integral equations are applied over a mesh sampling the concentrator volume such that a realistic representation of the continuous media emerges. The thermodynamic approach provides equations from which the photon chemical potential as a function of position within the concentrator may be determined by iteration. An optimal, self-consistent linearization of the depth dependence of the chemical potential for a single planar

concentrator that results in only analytic expressions has also been developed. This linearized 3D flux model [23] has been validated by comparison with the results of the original 3D flux model and, the linearization is accurate to within approximately 2% of the total luminescent intensities and peak values. Escape cone losses, absorption losses in the host material and re-absorption limit the efficiency of the luminescent concentrator and the thermodynamic models [12,13,19,20] allow the quantitative investigation of the luminescent species, the doping densities and the geometries that minimize these loss mechanisms.

Modeling large area devices has indicated the importance of top-surface losses that occur through the escape cone [24] both through primary emission and through emission of luminescence that has been reabsorbed and might otherwise have been trapped via total internal reflection or by mirrors. For an idealized, mirrored, QD doped 40cm LSC described in more detail in section 2.1.1, 78% of the luminescence is lost through the top surface. Recently, use has been made of wavelength-selective cholesteric liquid crystal coatings applied to the top surface in order to reduce these losses [25]. These focal conic cholesteric coatings are transparent to incoming light but reflect the emitted light. Initial experimental results [25] suggested that a significant increase in light output could be achieved by tuning the bandwidth of the coating. The thermodynamic approach may be used to quantify the effects of such coatings [24] by using the measured reflectivities of the liquid crystal coatings as the boundary conditions for the incident and luminescent light at the coated surfaces.

2.1.1 Idealized QD-LSC and top-surface losses

Thermodynamic modelling of an idealised, mirrored, 40×5×0.5 cm LSC doped with CdSe/ZnS QDs with emission matched to a GaInP cell (see Fig. 2(a)) indicates the importance of reducing top-surface escape cone losses.

The idealized LSC has perfect mirrors on one short and two long edges and the bottom surface, a perfectly transparent host material and a LQE of unity. The LSC absorption, incident AM1.5G spectrum and the average concentrated flux escaping the bare right-hand edge of the idealised LSC are illustrated in Fig. 2(b). Note that a logarithmic scale is necessary to compare the narrow concentrated escaping flux and the incident flux. This idealised LSC absorbs 24% of the incident photons in the AM1.5G spectrum.

The photon concentration ratio, C , which is the ratio of the concentrated flux escaping the right-hand surface of the LSC to the flux incident on the top surface, is 4.18. However, since the concentrated flux escaping the right-hand surface is a narrow-band matched to the spectral response of the cell it can all be converted and the idealized LSC would produce 8× the current compared to the cell alone exposed to AM1.5G. However, 78% of the luminescence is lost through the large top-surface area and only 22% may be collected at the right-hand surface. Therefore there is a need to reduce these large top-surface losses in order to design

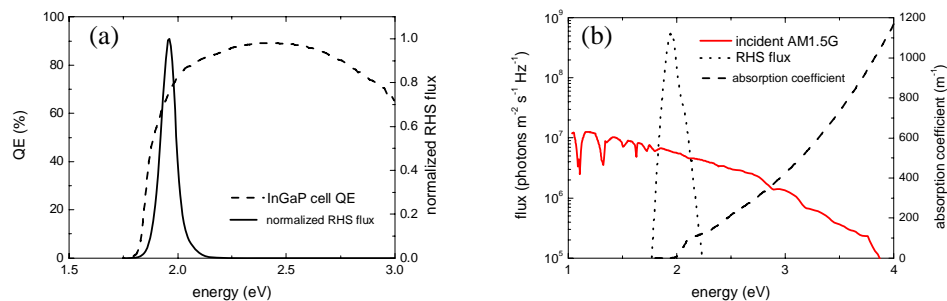


Fig. 2. (a) Quantum efficiency (spectral response) of the GaInP cell used in modelling the idealized LSC together with the modelled luminescence escaping the right-hand surface (RHS) of the LSC that would be coupled into the cell. (b) Absorption of the LSC material used in the calculations for the idealised system together with the flux incident on the top surface and the predicted concentrated average luminescent flux escaping the right-hand surface of the idealised LSC.

more efficient devices. An idealized notch filter on the top surface, which has a reflectivity of 99.9% in the notch (covering the luminescence between 1.8 and 2.2 eV) and a reflectivity of 0.01% everywhere else, would increase the output by almost a factor of 3.1. Such a top coating reflects a portion of the incident light before it can be absorbed in the LSC so the coated idealized LSC absorbs only 21% of the incident light but has a predicted photon concentration ratio of $C = 12.98$. Obviously real coatings do not have the idealized properties used in these predictions but these calculations serve to illustrate the maximum gains that could be achieved.

2.1.2 Test QD- and Dye- LSCs

Four test LSCs doped with QDs and dyes were characterized both with and without appropriate focal-conic cholesteric coatings [24] and with and without back surface air-gap 3M multilayer dielectric foil mirrors. The two QD doped test LSCs were comprised of PMMA doped with red and yellow CdSe/ZnS core-shell QDs purchased from Nanoco. The two dye doped test LSCs were approximately comprised of Plexit 55 (a commercially available polyacrylate) doped with red and yellow coumarin fluorescent dyes purchased from Bayer.

The absorption of the two QD samples is plotted in Fig. 3(a) together with the measured and modeled luminescence escaping the right-hand surfaces [24]. Fig. 3(a) shows the good agreement between the shape and position of the predicted and observed luminescence for both QD samples and the dye samples show a similar good agreement (see e.g. [12]). For these coatings the trough in the coating is highly angular dependent. The trough positions for each applied coating were tuned to give the maximum $\cos(\theta)$ weighted overlap integral between the reflectivity ($R \sim 1-T$) of the coating and the luminescence of each test LSC. Fig. 3(b) shows the angularly averaged reflectivity of one coating appropriate to the luminescence and that at normal incidence appropriate to the incident light stream.

Short circuit currents, J_{SC} , resulting from the radiation escaping the right-hand surfaces of the dye and QD doped test LSCs, both with and without the coatings (tested on the top and bottom surfaces) and with and without a 3M multilayer dielectric foil back surface air-gap mirror, were measured and compared with the values predicted by the thermodynamic model [24]. The air gap mirror conserves total internal reflection at the bottom surface. The model and predictions showed good agreement for all four test concentrators and the results for the red dye concentrator are illustrated in Fig. 4.

Unfortunately the cholesteric coatings tested led to a predicted reduction in output owing to both coating transmission losses and reflection of the incident light by the coatings before it could be absorbed. This was not compensated for by the increase in trapping of the luminescent light inside the test LSCs by the coatings. The increase in trapping was seen in the models through a higher average photon chemical potential [24]. Cholesteric coatings with much reduced transmission losses are now available and will be evaluated in the near future.

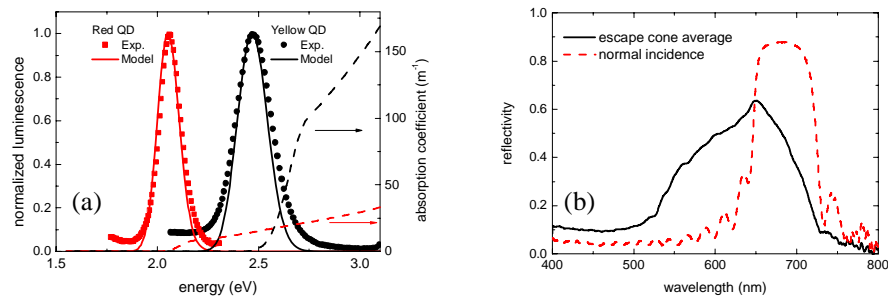


Fig. 3. (a) Measured absorption coefficient together with the normalized predicted and observed luminescence escaping the right-hand surfaces of the 5mm thick test LSCs doped with red and yellow CdSe/ZnS QDs. (b) Reflectivity of one right-handed cholesteric coating at normal incidence and averaged over the escape cone.

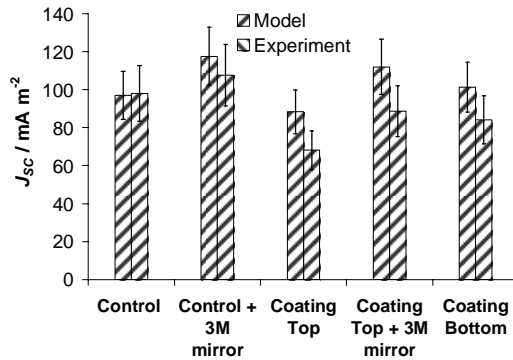


Fig. 4. Measured and predicted short-circuit currents, J_{sc} , for the red dye doped test LSC.

The model results for the dyes agreed with the measurements using the known LQE of 0.95 for both dyes giving confidence in the fitted $LQEs$ of 0.45 and 0.50 for the red and yellow QDs respectively [24]. The results show that the thermodynamic approach can predict both the room temperature red-shift and the total flux escaping each surface of the LSC providing a tool for its optimisation.

2.2 Ray trace modeling

Ray-tracing for LSCs uses basic ray-tracing principles, which means that a ray, which represents light of a certain wavelength travelling in a certain direction, is traced until it leaves the system e.g. by absorption or reflection at the interface. The model applies statistical averaging of the absorption, leading to a much reduced computation time, compared with modeling of individual luminescent particles or dyes, such as in the work of Gallagher [17]. The main extension to the standard ray-tracing model is the handling of the absorption and emission by the luminescent species in the LSC. The 3-D ray-tracing program described here takes these absorption and emission characteristics into account [26].

The model is well able to explain experimental results on practical LSC devices of reflection and transmission measurements, as well as LSC photo response [26]. Also, a parameter study has been performed to find attainable LSC efficiencies. The parameters studied were 1) mirror configuration; 2) polymer material properties; 3) solar cell type; 4) dye type. In addition, the major loss factors could be determined.

2.2.1 Mirror configuration

The basic configuration for the modeling in this section consists of a planar $5 \times 5 \text{ cm}^2$ luminescent concentrator with mirrors on the three side facets and a mc-Si cell on the remaining side facet as well as a mirror at the bottom (see Fig. 1). The concentrator consists of a PMMA plate (refractive index $n=1.49$, absorption 1.5 m^{-1}) doped with two luminescent dyes, CRS040 from Bayer and Lumogen F Red 305 from BASF, with a FQE's of 95% [27]. With the ray-tracing model the efficiency of this basic configuration was determined to be 2.45%.

Next, the mirror configuration was varied, using a realistic FQE of 95% for both dyes. Direct mirrors or a mirror with an air-gap between the mirror and the LSC were modeled, as well as different reflectivity values and specular or Lambertian mirror types. Without a side mirror, rays within the escape cone are leaving the LSC at the side; rays outside the escape cone are subject to total internal reflection, see Fig. 5(a). When a direct mirror is applied, the total internal reflection would disappear, and all rays would reflect with the reflection coefficient of the mirror, see Fig. 5(b). For the rays outside the escape cone this leads to a reduction in the reflection, and thus lower power conversion efficiency. The use of an "air-gap mirror", i.e., an air-gap between the mirror and the LSC, combines total internal reflection with reflection of the escaping rays, see Fig. 5(c). The results of the ray-tracing calculations

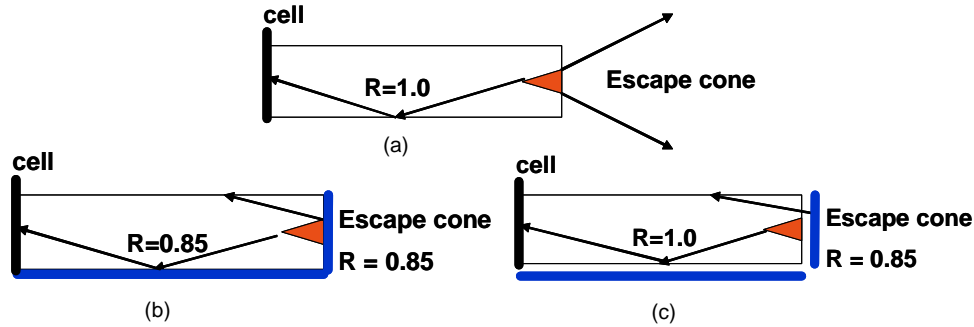


Fig. 5. Different mirror configurations that are used in the ray-tracing simulation. (a) no mirrors, (b) direct mirrors, and (c) air-gap mirrors.

show a maximum efficiency of 2.94% for the case with 97% reflective air-gap mirrors (e.g. 3M adhesive visible mirror foil, with a reflection of 97%) at the sides and a 97% reflective Lambertian air-gap mirror (e.g. standard integrating sphere material with a reflection of 97%) at the bottom.

2.2.2 Polymer material properties

In a similar manner the background absorption of the polymer was varied in the absorption and emission range of the dye from the current value of 1.5 m^{-1} to a value of 10^{-3} m^{-1} , which can be obtained in PMMA based polymer optical fibres [28]. The result is shown in Fig. 6, where the best, realistic mirror configuration was used, i.e., a 97% Lambertian reflecting air-gap bottom mirror and 97% specular reflecting air-gap side mirrors: the efficiency of the LSC can be increased to slightly over 3.4%.

An additional increase of the refractive index of the polymer from 1.49 to 1.7 would result in an increase in η to almost 3.8%, as a result of the fact that a higher refractive index leads to a larger fraction of the emitted dye luminescence being trapped in the concentrator plate. Note, however, that a polymer with the combination of a refractive index of 1.7 and an optical absorption of 10^{-3} m^{-1} is not available at this moment.

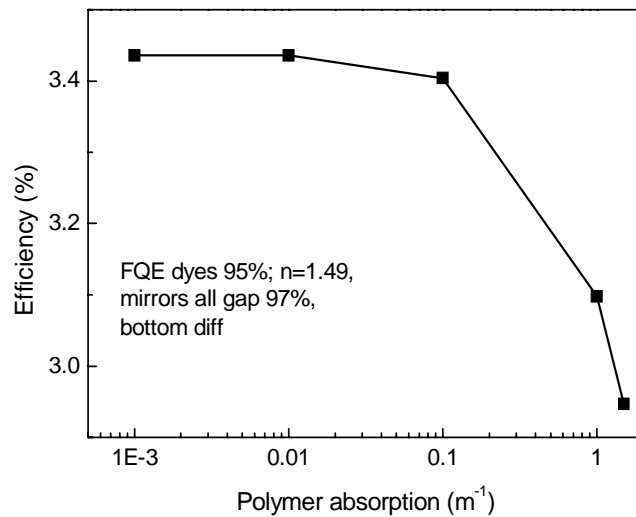


Fig. 6. Influence of the background absorption of the polymer LC plate on the current collected from the mc-Si solar cell.

2.2.3 Solar cell optimization

One major reason for the lower efficiency compared to the work of Zastrow [29] is that the solar cells that are used up to now are not optimized for the emission-spectrum of the dye: mc-Si solar cells absorb all the light up to about 1100 nm, but the dyes used in these LSCs emit around 650 nm. It would therefore be beneficial to use a solar cell with a larger bandgap, because these deliver the same current as the mc-Si cell, but at larger V_{oc} 's. In Table 1 estimates are listed for attainable efficiencies η for similar concentrator plates with different solar cells attached. Replacing the mc-Si cell by a GaAs cell or a InGaP cell, will increase η from 3.8% to 6.5 and 9.1%, respectively (based on V_{oc} (FF) values of 0.58 V (0.83), 1.00 V (0.83), and 1.38 V (0.84), for mc-Si, GaAs, InGaP, respectively). Thus, the use of GaAs or InGaP cells will result in higher efficiencies, but these cells are more expensive. A cost calculation must be performed to determine if the combination of the luminescent concentrator with this type of cells is an interesting alternative to mc-Si based solar technology.

Table 1. Calculated efficiencies (in %) for the LSC based on experimentally determined parameters and subsequently using optimized parameters based on realistic estimates

mc-Si	GaAs	InGaP	parameters
2.4	4.2	5.9	fixed mirrors, 85% reflectivity, dyes with 95% FQE
2.9	5.1	7.1	97% reflectivity "air-gap mirrors" on sides, and 97% reflectivity Lambertian mirror at bottom
3.4	5.9	8.3	reduce background absorption of polymer matrix from 1.5 m^{-1} to 10^{-3} m^{-1}
3.8	6.5	9.1	increase of refractive index from 1.49 to 1.7

2.2.4 Extending the spectral sensitivity range

Instead of using an optimized solar cell, a dye could be added that absorbs into the infrared. However, such dyes have not yet been developed, i.e. their FQEs are too low for use in an LSC, while absorption spectra are suitable. Zastrow [29] already addressed this in the 1980s, and argued that the C-H bond vibration becomes resonant with the luminescent transition in the dye, providing a non-radiative pathway for the excitation resulting in quenching of the luminescence. Nevertheless, despite the low FQE, the IR dyes can improve the efficiency when used in stacked concentrators [30]. Ray-tracing calculations show that adding an IR dye with an FQE of 50% to a plate containing both Red305 and CRS040 dye, results in a reduction in efficiency from 3.8 % to 2.3%, see Table 2. This is due to the fact that the emission from the Red305 dye is now absorbed by the low FQE IR dye, thereby increasing the re-absorption losses substantially. However, if the IR dye is present in a separate LSC plate below the plate with the Red305 and CRS040 dyes, the efficiency can increase by about 20% compared to a single plate containing the Red305 and CRS040 dyes, but at the expense of increased material and solar cell costs. Putting the IR dye containing plate at the top is less efficient, due to the filtering effect of the top plate: photons that are otherwise efficiently converted by the CRS040 and Red305 dyes are absorbed by the IR dye.

Table 2. Ray-tracing results for a stack of two LSC plates with a low FQE IR dye in one plate and the Red305+CRS040 dyes in the other, compared to all dyes in a single LSC plate

dye // cell combination	efficiency (%)
single plate Red305+CRS040 // 1 c-Si solar cell	3.8
single plate Red305+CRS040+IR dye // 1 c-Si solar cell	2.3
stack Red305+CRS040 top/IR dye bottom // 2 c-Si solar cells	4.5
stack IR dye top/Red305+CRS040 bottom // 2 c-Si solar cells	4.3

If an IR dye with an FQE of 95% could be synthesised, this dye combined with the CRS040 and Red305 dyes in a single LSC plate would lead to an increased efficiency of 5.4%. When comparing this efficiency with the efficiency that can be achieved by using GaAs or InGaP cells it can be concluded that the use of a different solar cell is more beneficial than the use of a high FQE IR dye. However, as these cells are more expensive, cost calculations must be performed to see which option is most favourable.

2.2.5 Major losses

The LSC with two dyes and an η of 3.8% as mentioned above has an EQE of 50-60% in the absorption range of the dyes used. The remaining part of the light is mainly lost at the top surface. It is clear that further improvement of the LSC must be achieved by reducing the top escape losses. One way of doing this is to use special top mirrors that transmit light in the dye absorption range and reflect light in its emission range, so-called wavelength selective mirrors. The mirror should be transparent in the region where the dye is absorbing and highly reflecting in the range where the dye is emitting. The absorption and emission spectra of the dye are shown in Fig. 7(a), together with the desired transmission and reflection spectrum of the mirror. As described earlier one way to realize such a mirror is by applying selectively-reflective chiral nematic (cholesteric) liquid crystal (LSC) layer(s) [25]. In Fig. 7(b) the optical properties of cholesteric layers are illustrated.

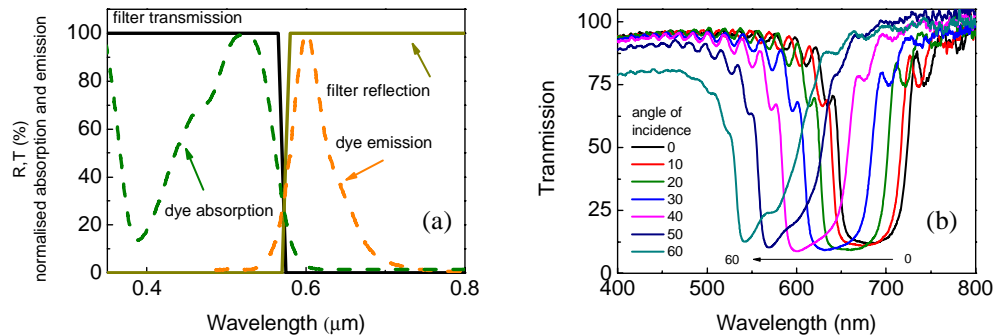


Fig. 7. (a) Absorption and emission spectra of the Red 305 dye, together with the desired transmission and reflection spectrum of the selective mirror; (b) reflection of a cholesteric layer for different angles of incidence. With increasing angle of incidence the centre wavelength of the high reflection region moves to shorter wavelengths.

As can be seen, the transmission shows the desired low transmission in the dye emission range, but the transmission band is rather small and shows interference fringes. Furthermore, the transmission spectrum depends on the angle of incidence. This will have a large impact on the application of such a mirror in the LSC. The emission by the dye is more or less random and will thus arrive at the top interface under various angles of incidence. So a ray at a wavelength of 600 nm at normal incidence will not be reflected, as the center wavelength of the cholesteric mirror at this wavelength is 680 nm, but would it have an angle of 40° it would be reflected, see Fig. 8(a). To determine the effect of such a cholesteric mirror, the reflection and transmission characteristics of Fig. 7(b) were implemented in the ray-tracing program [31]. Calculations were performed for an LSC with and without a cholesteric mirror. Fig. 8(b) shows the current from the attached solar cell, as calculated with the ray-tracing program for different center wavelengths of the cholesteric mirror. The calculations were done for the configuration with a diffuse air-gap mirror at the bottom and for a direct 100% reflecting specular mirror at the bottom. From Fig. 8(b) it is clear that the center wavelength of the cholesteric mirror needs to be red-shifted substantially for optimal performance. Although the peak emission wavelength of the dye is about 600 nm, the optimal center wavelength of the

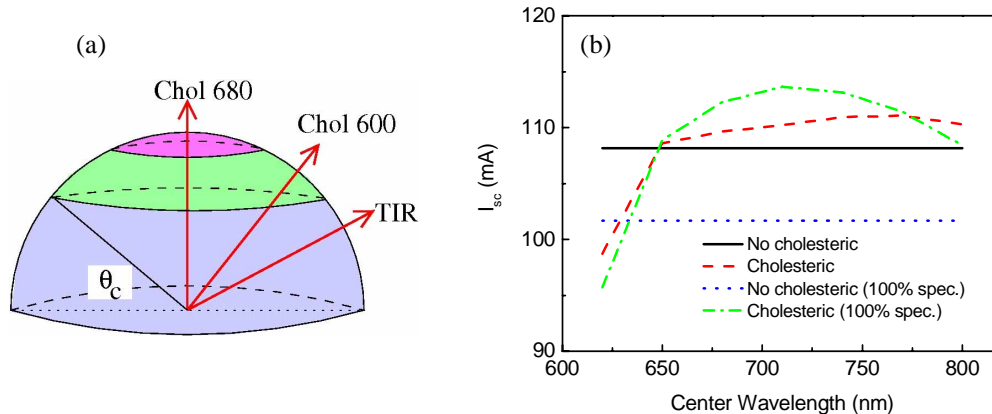


Fig. 8. (a) Schematic view of the different regions the emitted fluorescence of the dye is facing when a cholesteric mirror with a center wavelength of 680 nm is applied. Light that falls perpendicularly on the top surface faces a reflector with a center wavelength of 680 nm, whereas light that falls in at roughly 45° faces a reflector with a center wavelength of 600 nm. At even larger angles total internal reflection will take place. (b) Calculated short circuit current from the mc-Si cell connected to the LSC plate as a function of the center wavelength of the cholesteric top mirror as compared to the situation where no top mirror is applied. Calculations are shown for a diffuse air-gap bottom mirror, and a direct specular bottom mirror (100% spec.).

cholesterics for normal incidence is 710 nm. Furthermore, the effect of the cholesteric mirror is much larger, 12%, in the case of a direct 100% reflecting specular mirror than for the diffuse air-gap bottom mirror, 3%. The reason for this must be found in the different angular dependence of the reflected rays. In the case of a diffuse air-gap mirror, the randomly emitted luminescence is scattered at the backside mirror and a fraction of this scattered light will be transported directly to the solar cell, without reaching the top surface. This fraction will not benefit from the application of a cholesteric top mirror. With a direct specular mirror, the randomly emitted luminescence will be specularly reflected and will thus remain randomly oriented. As a result, part of the emission will reflect at the backside and escape from the top side, if emitted within the escape cone. For this reason, the performance of a direct specular bottom mirror is lower than for a diffuse air-gap mirror. However, by applying a cholesteric mirror, now the escaping light will be reflected and the light can reach the solar cell.

The subject of selective mirrors has recently been addressed by several other groups [24,32,33] and is clearly an important topic in the study of LSCs. Escape cone losses through the top surface of the LSC may also be reduced by exploiting directional emission within the LSC. Organic dye molecules can be aligned using liquid crystalline host materials [34], and nanorods self-align at high concentrations and may also be aligned by stretching polymer films. The dye alignment must be chosen such that the peak in the emission direction falls outside the escape cone of the LSC. However, this will also reduce the absorption in the waveguide for perpendicular incidence light. Thus, it is expected that the dye concentration must be increased. On the other hand, Debije *et al.* [34] suggest to use a high concentration dye layer with a transparent waveguide on top. In this configuration, the emitted light will mainly pass through the transparent waveguide. After reflection at the top surface it will have an almost 90 degrees angle with respect to the dyes and reabsorption losses will thus be strongly reduced. This results in a larger fraction of the luminescent light being guided in the direction of the attached solar cell.

2.3 Comparison of modeling approaches

The modeling methods described above should yield preferably identical results, when modeling identical LSCs. The thermodynamic approach requires a minimum of input data and is quick to run, but it is limited to rectangular flat plate LSCs homogeneously doped with a

single luminescent species. The ray-trace approach is more flexible allowing multiple dopants, thin-films and different geometries to be investigated. In order to check the validity of both model approaches, four Plexit slabs, of different sizes, containing a Bayer Fluorescent Red Coumarin dye or a Fluorescent yellow Coumarin dye were fabricated [12], and modeled. The dimensions of each slab are given in Table 3. The quantum yield of both dyes was determined to be 0.95. To measure the electrical output of each, the slabs were illuminated at normal incidence by an Oriel fibre-optic lamp. A 2.65×2.65 mm Siemens Si photodetector was utilised to obtain short circuit current (J_{sc}) values at the edge of each slab. Ray-trace modeling and thermodynamic modeling, as described above, were used to predict the photon count and luminescence spectrum escaping at the edge where the photodetector was placed. The photodetector spectral response and its angle dependent reflectivity were used with the predicted photon count to obtain the predicted J_{sc} of the four LSC devices, as given in Table 3. Clearly, there is a high level of agreement between the predictions and observed values. Despite the many differing processes involved in each modeling approach, there is very good agreement between both techniques. The results show that both thermodynamic and ray-trace modeling provide useful tools for optimizing LSC devices and predicting their electrical output.

Table 3. Measured and predicted short-circuit current densities (J_{sc}) of the four LSC devices

slab	dimensions (cm ³)	measured J_{sc} (mA/m ²)	predicted J_{sc} (mA/m ²)	
			Thermodynamic	Ray-trace
Red large	4.78×1.7×0.255	53.2 ± 2.0	51.6	51.9
Red small	1.93×0.994×0.25	22.5 ± 2.0	23.9	24.9
Yellow large	4.78×1.78×0.269	10.4 ± 2.0	10.2	9.3
Yellow small	2.26×1.0×0.27	5.2 ± 2.0	5.0	5.0

2.4 Device geometry effects

The effect of varying the device geometry on LSC performance can be analyzed using ray-trace modeling. Square, right-angled triangular and hexagonal quantum dot doped luminescent solar concentrators (QDSCs) of increasing top surface apertures (A_{conc}) were considered. Concentration ratios (C) were predicted for increasing A_{conc} of each geometry type, as detailed in [35]. Figure 9 shows that a hexagonal geometry attains the highest C for the range of A_{conc}

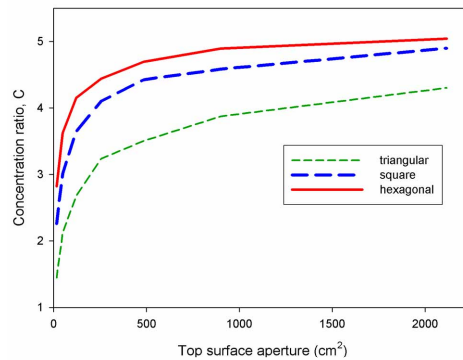


Fig. 9. Predicted concentration ratios (C) for devices of varying geometry and top surface aperture (A_{conc}). The device thickness was fixed at 0.3 cm.

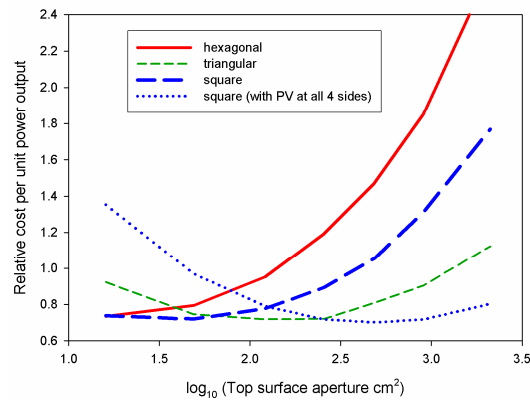


Fig. 10. Predicted *relative* costs per unit power output for square, triangular and hexagonal QDSC geometries of increasing top surface aperture. The predictions for square QDSCs with PV attached at all four sides [35] are also shown.

considered. However, for a given A_{conc} , each geometry type has a different area of attached PV (A_{pv}). Also, the cost of materials of the LSC plate, although much lower than the cost of PV (per m^2), is not negligible. Therefore, to determine the optimum geometry, relative costs per unit power output were calculated, as detailed in [35], with the relative costs of the LSC plate and PV factored in. The relative power output of each device is assumed to be proportional to the product of the concentration ratio attained and A_{pv} , in each case. The results, shown in Fig. 10, indicate that all geometries can attain the same minimum relative cost per unit power. Under the assumptions made, it is concluded that varying the geometry *type* does not offer any significant relative cost reduction, however, the results do show that the selection of device *size* is critical for achieving the lowest possible cost per unit power output.

3. Experimental work

3.1 Preparation of samples

Since acrylic polymers are known to have the potential for high optical transparency, considerable stability and good mechanical properties, our efforts to make LSCs were focused on this class of polymers. Two main kinds of samples containing luminescent molecules or particles were prepared: polymer plates and coatings on substrates.

3.1.1 Plates

Plates were produced by polymerisation of monomers or monomer mixtures in flat cuvettes. The monomer systems used in most cases were methylmethacrylate (MMA), methylmethacrylate/2-hydroxyethylmethacrylate (HEMA) with MMA:HEMA=1:1 by weight, Plexit 55, and mixtures of dodecylmethacrylate(laurylmethacrylate(LMA)) with MMA and ethylenglycoldimethacrylate (EGDM). The MMA (>99%, Merck Schuchardt) used to make PMMA plates contained a stabilizer, but better results were obtained using distilled MMA. The prepolymer Plexit 55 is a commercially available viscous MMA/PMMA mixture containing 30-40% polymer (Röhm GmbH). The purities of the monomers HEMA (Merck Schuchardt), LMA (Aldrich) and EGDM (Fluka) were 97% , 96% and > 97%, respectively.

The cuvettes consisted of 3-4 mm thick glass plates with an elastic distance holder between the plates, which were held together by steel clamps. As the polymer sometimes was sticking strongly to the glass after the polymerization reaction, it may be advantageous to use glass with a surface coating that diminishes adhesion. Silicon rubber bands of 3mm, 5mm or 8mm thickness or FEP tubes of 3mm, 5mm or 10mm diameter were used as inert distance

holders. The distance holders as well as the clamps must be elastic to compensate the considerable shrinkage of the polymerizing material in the cuvette. These elastic properties of the cuvettes together with certain adhesion between glass and polymer allowed to avoid undesirable partial separation of the still reacting, solidifying polymer material from the glass leading otherwise to irregular LSC surfaces.

The reaction mixtures were polymerized by means of thermally or UV initiated polymerization, respectively. Plexit and MMA were polymerized in most cases thermally using 0.05% - 0.1% azoisobutyronitrile (AIBN) as initiator, whereas plates on the basis of MMA/HEMA or other copolymer mixtures were usually made by UV polymerization using in many cases the liquid initiator Irgacure 1700 (Ciba). Plexit was polymerised for 20 hours in an oven using a temperature program with a maximum temperature of 70°C. For MMA best results were achieved for polymerization in a bath with circulating water of 50°C (about 20 hours). The thus thermally produced plates contained still up to 9% monomer, but after a post-treatment at 110-120°C for some hours no remaining monomer was present, as evidenced by infrared spectroscopy. In a number of experiments the distilled MMA was prepolymerised before filling it into the cuvette: the strongly stirred MMA plus 0.1% AIBN initiator was heated to 95°C with the flask being purged by nitrogen. After ~20 minutes the then viscous liquid was very rapidly cooled in ice to stop the reaction.

For UV polymerization the cuvettes were irradiated from two sides by UV-A radiating lamps (band maximum 360nm). The intensity of the irradiation applied was different for the various mixtures and had to be tested out. For 3mm thick P(MMA/HEMA) plates, e.g., at very low UV intensity a polymerization time of about 2 hours was sufficient.

The reaction mixtures were prepared by solving the initiator and the dye in the monomer, if possible, or in a small amount of a solvent compatible with the monomer with this amount being then added to the monomer. The reaction mixtures were degassed before starting polymerisation to avoid formation of bubbles in the plates.

Following the above procedure, clear, transparent, bubble-free plates with even surfaces were obtained with best loss coefficients achieved being in the order of 0.5m^{-1} (for plates without dye). Common plate sizes were, e.g., $10\times 10\text{ cm}^2$ and $15\times 15\text{ cm}^2$, with the maximum size produced being about $50\times 20\text{ cm}^2$.

3.1.2 Coatings

Coatings were prepared by casting solutions of PMMA, ethylmethacrylate polymer (Paraloid B72, Fa. Dr. Georg Kremer) or cellulose triacetate (CTA) on glass or Plexiglas substrates of $5\times 5\text{ cm}^2$ size. Substrate thicknesses were 1 mm or 3 mm. Suitable solvents had to be chosen depending on the polymer and the dyes or nanoparticles. Paraloid B72 was dissolved in ethyl-acetoacetate (AEEE), solvents used for PMMA were ethyl-acetoacetate or CHCl_3 , and CTA was dissolved in a $\text{CHCl}_3/\text{CH}_2\text{Cl}_2$ mixture. Stock solutions of the polymers (e.g. 10% PMMA/AEEE) were made to which the luminescent species was added (sometimes after dissolving it in a small amount of pure solvent) with dispersing it thoroughly by stirring or, if necessary, by means of ultrasound until the mixture was clear. In most cases definite amounts of solution, resulting in roughly reproducible layer thicknesses, were poured out onto the substrate and dried for 12-24 hours at 20°C. The drying procedure had to be tested out for the different solvents, in some cases it was necessary to slow down the evaporation rate to obtain clear coatings with an even surface. Remaining solvent was driven out by storage at higher temperatures (~80°C). Depending on polymer concentration and solution amount used coatings with thicknesses between $< 10\mu\text{m}$ and several hundred μm were prepared.

3.1.3 Luminescent species

As luminescent species a number of organic dyes as well as some types of nanoparticles (quantum dots, nanorods) were used. An overview of the most important dyes used is given in table 4. The suppliers of the dyes were BASF (Lumogen dyes), Bayer AG (Macrolex Fluorescence Red G), Radiant Color N.V. (CRS040) and Lambda Chem GmbH (S13), part of S13 was a gift from Prof. Langhals (LMU Munich).

Table 4. Overview of used dyes, their absorption and luminescent emission peak wavelengths and luminescent quantum yields

dye	chemical structure	absorption λ_{\max} (nm)	emission λ_{\max} (nm)	quantum yield (%)	reference
Lumogen F Blue 650	Naphtalimide	377	411	>80	[36]
Lumogen F Violet 570	Naphtalimide	378	413	94	[36]
Lumogen F Yellow 083	Perylene	476	490	91	[36]
Lumogen F Yellow 170	Perylene	505	528	>90	[36]
Lumogen F Orange 240	Perylene	524	539	99	[36]
S13	Perylene	526	534	100	[37]
Lumogen F Red 305	Perylene	578	613	98	[36]
Macrolex Fluorescence Red G	Coumarin	520	600	>80	[26]
				87	[27]
CRS040 (new: CFS002 Yellow)	Coumarin	440	506	98	[27]

A number of tests was performed using two types of commercially available quantum dots (SD 387, SD 396 from Nanoco), but most work was done with multishell CdSe/CdS/CdZnS/ZnS quantum dots from Utrecht University [38,39]. Furthermore CdSe/ZnS nanorods from L. Manna's group [40] were used. The preparation of acrylic polymer plates of good quality containing nanoparticles by polymerization as described above was more complicated than found with organic dyes. This is due to the fact that the QDs are passivated by hydrophobic ligands, which causes the nanoparticles to form turbid dispersions in the hydrophilic monomers (e.g. MMA) and/or solvents often used. The luminescence of the hydrophobic nanoparticles in inappropriate, e.g. hydrophilic, media was quenched as a consequence of the formation of agglomerates and resulting energy transfer between the QDs. However, when the more hydrophobic monomer LMA was used, clear nanoparticle/LMA/EGDM/initiator mixtures could be prepared, which were polymerized successfully. As a result highly transparent and strongly luminescent plates containing QDs or nanorods with sizes of up to about $5 \times 5 \times 0.4 \text{ cm}^3$ were prepared.

3.2 Dye-doped LSCs

Based on the modeling results presented in Section 2.2, experiments were performed to verify model predictions. Initially only one luminescent dye, Red305, was used in the LSC. Because Red305 captures only a small region of the solar spectrum it is combined with the blue absorbing dye CRS040. This LSC plate was connected to a high efficiency mc-Si cell (18.6%) using microscope immersion oil; the side mirrors consisted of a 98% reflective visible mirror foil. Both the higher efficiency of the mc-Si cell and the high reflectivity of the mirror foil contribute to an increase in the EQE as can be seen in Fig. 11. Adding the CRS040 to the Red305 dye (black line), gives an additional increase in the EQE and a slight improvement in the spectral sensitivity around 370 nm. Based on these EQE spectra the AM1.5 short circuit current can be calculated. The result is shown in Table 5. The LSC devices were also measured using the ECN solar simulator, resulting in measured AM1.5 efficiencies of 2.4% for the Red305 doped LSC and 2.7% for the Red305/CRS040 doped LSC. These efficiencies are comparable to the efficiency obtained with ray-tracing simulation as shown in Table 5.

To verify the effect of a selective top mirror a commercially available dichroic mirror having the desired characteristics was used instead of a cholesteric mirror, because the latter was not available. The reflection and transmission spectrum of this mirror (LOT-ORIEL 590FD24-50SX) is shown in Fig. 12. The mirror was employed in combination with an LSC for different types of attached solar cells, i.e. mc-Si, GaAs, and InGaP. The results of external quantum efficiency (EQE) measurements are shown in Fig. 13. For all solar cells used the

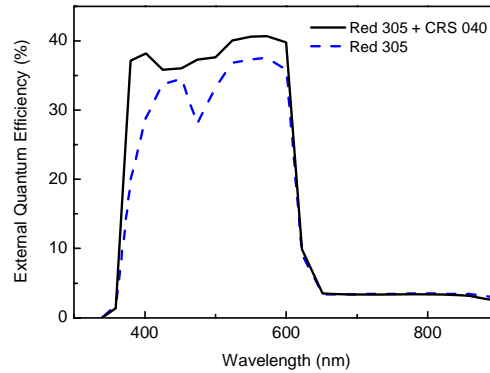


Fig. 11: External quantum efficiency of an LSC with mc-Si solar cell, with one or two dyes dispersed in the polymer matrix.

Table 5. Calculated AM 1.5 short circuit current (I_{sc}) and power conversion efficiency, together with the measured efficiency using the ECN solar simulator. The efficiency of the used bare Si cell was 18.6%.

LSC plate	Calculated I_{sc} (mA)	Measured I_{sc} (mA)	Calculated efficiency (%)	Measured efficiency (%)
Red305	138	133	2.5	2.4
Red305+CRS040	153	147	2.8	2.7

EQE shows an improvement in the dye absorption range when the mirror is applied (note that the lower EQE for the InGaP cell is due to a bad electrical contact of the cell). However, the EQE spectrum without the filter is somewhat broader, indicating that the cut-off wavelength of the mirror is too blue-shifted, contrary to what could be expected based on the spectra in Fig. 7, where it seems to be slightly too red. The reason is that this dichroic mirror, similar to the cholesteric mirror, shows an angle of incidence dependent reflection and transmission spectrum. As discussed in Section 2.2.5 for the cholesteric mirror, the cut-off wavelength of the dichroic mirror should be red shifted for optimal performance.

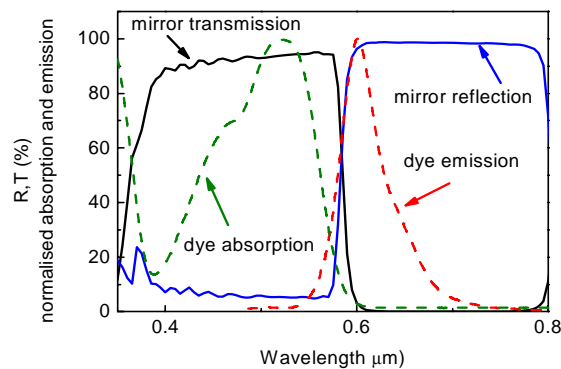


Fig. 12. Absorption and emission spectra of the Red305 dye, together with the transmission and reflection spectrum of the LOT-ORIEL mirror.

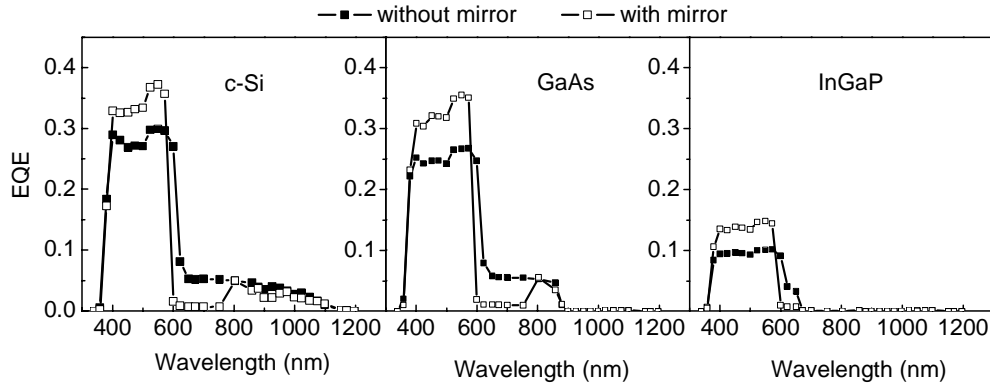


Fig. 13. External quantum efficiency of LSC solar cell combinations comparing the case with and without mirror.

The shoulder at wavelengths above 600 nm in Fig. 13 for the case without the mirror is resulting from light that enters the plate and that is not absorbed by the dye. This light is scattered at the diffuse rear-side mirror and part of it will reach the solar cell, before it leaves the LSC at the top. When the mirror is applied, light incident on the LSC at these wavelengths will be reflected at the top and will thus not enter the plate. As a result, this shoulder disappears in the EQE spectra with the mirror. Above 800 nm the filter becomes partly transparent again and a small EQE response can be observed. The relative contribution of the diffusely scattered light compared to the dye contribution is rather large for the LSC with a mc-Si cell, but decreases for the GaAs and InGaP cells due to the wider bandgap of these materials. The contribution will also decrease if larger LSC plates are used. It can thus be concluded that the dichroic mirror will only result in an increased performance for large, $> 25 \text{ cm}^2$, LSC plates and for smaller LSC plates only when an InGaP cell is connected.

3.3 Stability issues

The long-term stability of LSCs against environmental influences is a very important issue, since their expected useful life is usually set to at least several years. This request refers to the luminescent dyes or particles as well as to the polymer matrix material. Whereas some otherwise suitable looking polymers must not be taken into account due to this requirement, acrylic polymers can be made very stable against environment; recently a stability guarantee of 30 years is granted by one supplier for some PMMA products. Therefore the main problem is the stability of the luminescent components of the LSC. The degradation rates of organic dyes in a polymer matrix are strongly dependent on minor components, which may be present in the LSC, e.g. monomer remainings, stabilisers, initiators and other additives. Hence greatly varying stabilities were found for a number of dyes incorporated into various polymer plates (made by polymerisation) or into coatings made by casting [41].

Figure 14(a)-(c) shows the absorption spectra of an LSC doped with Red305. The spectra were taken at various intervals during illumination under a sulphur lamp (roughly 1/3 sun intensity in the spectral range of the dye), as well as under outdoor conditions. Also shown are the absorption spectra of a reference plate that was stored in the dark. As can be seen, Red305 seems to be quite stable in these plates. The reference shows no degradation and only minor bleaching of the dye is observed under the sulphur lamp as outdoors. At the same intervals, EQE spectra were taken. The result is shown in Fig. 14(d)-(f). The shape of the EQE spectra remains more or less unchanged. As shown in Fig. 15, the reference plate shows no or only minor degradation, whereas the plate aged under illumination by the sulphur lamp and under outdoor conditions shows a decrease in EQE of about 20%. The decrease when illuminated with a sulphur lamp seems to be faster than under outdoor conditions, but one has to keep in mind that the illumination under the sulphur lamp is continuous, whereas outdoor a day/night

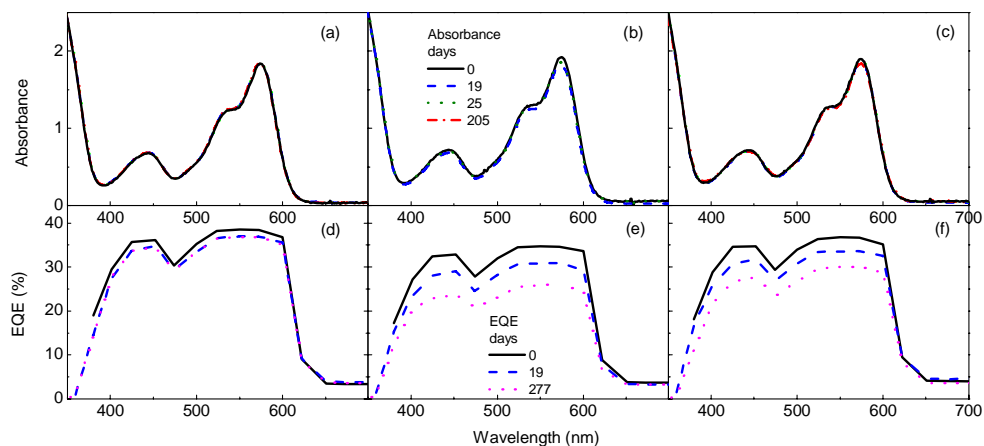


Fig. 14. Absorbance (a,b,c) and External Quantum Efficiency (d,e,f) spectra of Red305 doped LSC plates, taken at various intervals during (a,d) storage in the dark, (b,e) continuous illumination under a sulphur lamp, and (c,f) outdoor conditions.

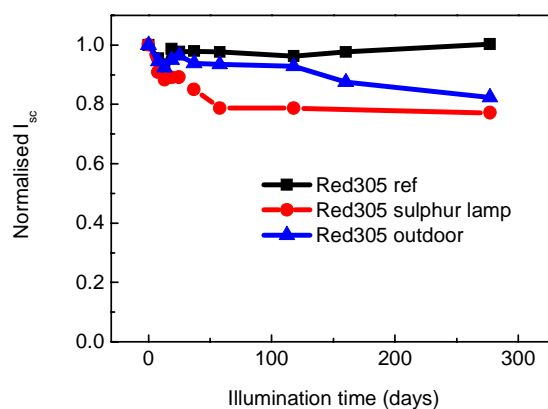


Fig. 15. Calculated I_{sc} at various intervals during aging.

cycle is present. Despite the fact that no change in absorption is observed during illumination, the EQE, and thus the I_{sc} , does show a decrease. This means that the dye is absorbing the same amount of light, but less light is reaching the solar cell, either due to a reduction of the luminescent quantum efficiency of the dye or due to an increased loss of the emitted light on its way to the solar cell. The latter has been observed by Seybold *et. al* [42] for perylene dyes. Within the measurement error, the absorption measurements on Red305 do not show an increase in the absorption in the emission range of the dye. However, due to the long path length of the emitted luminescence before it reaches the solar cell, a small increase in absorption, either due to the light-induced conversion of the luminescent dye into a non-luminescent one or due to a change in the matrix material, can lead to a noticeable reduction in EQE. From this it can not be concluded which of the two processes is responsible for the reduction in EQE.

Figure 16 shows the absorption spectra of a CRS040 and Red305 doped LSC plate during the ageing. The reference plate that was kept in dark is stable for the duration of the experiment, but the plate that was aged under the sulphur lamp, shows severe bleaching in the spectral range between 350 nm and 500 nm. This is the region where CRS040 is absorbing. The absorption band of Red305 between 500 nm and 600 nm remains almost unchanged, apart from a small decrease in the spectrum due to the disappearing absorption tail of CRS040.

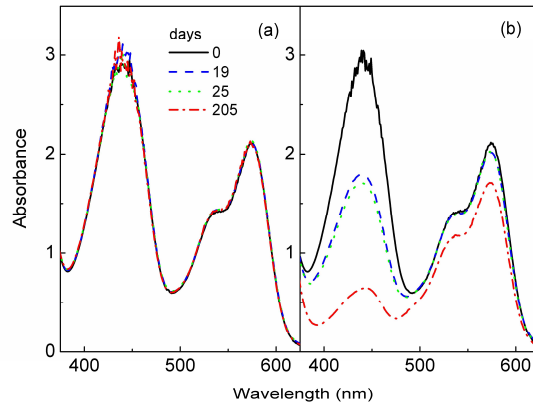


Fig. 16. (a) Absorbance spectra of CRS040/RED305 doped LSC plates, taken at various intervals during (a) storage in the dark, (b) continuous illumination under a sulphur lamp.

For comparison an LSC doped with only CRS040 was aged simultaneously. The absorbance spectrum of this LSC plates reduced in 46 days to about 50% of the initial absorbance during the ageing. This reduction in absorbance is comparable to the reduction seen in the plate with both CRS040 and Red305 demonstrating the instability of CRS040.

To study the mechanism of the degradation of the dyes in more detail, monochromatic light ageing experiments were performed. In these experiments, high intensity LED light was used to illuminate the LSC plates only in the absorption band of one of the dyes. Figure 16 shows the effect of illuminating a Red305 doped plate at 470 nm, i.e. within the absorption band of CRS040, or 589 nm, corresponding to the absorption band of Red305. For both excitation wavelengths, the absorption of the plate remains unchanged after 631 hours of illumination. The same experiment was performed on an LSC doped with both Red305 and CRS040. As can be seen in Fig. 17, illumination at 589 nm does not induce degradation, but illumination at 470 nm induces severe bleaching of the CRS040 absorption band, as was also observed under white light illumination (see Fig. 16). Contrary to the general understanding that UV light is responsible for the bleaching of organic dyes, this experiment shows that bleaching of CRS040 is also induced by 470 nm light.

A series of LSC plates without solar cells was positioned on the roof (facing south at 45° tilt angle) of the FhG-IAP in Germany for more than 2 years. The plates were fabricated using different luminescent dyes and matrix material. From time to time the absorption of the plates

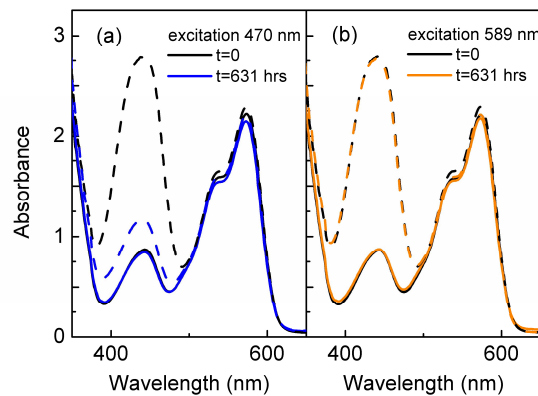


Fig. 17. Absorbance spectra of a CRS040/Red305 (dashed lines) doped LSC plate and Red305 only (solid lines) doped LSC plate before and after monochromatic light illumination at (a) 470 nm and (b) 589 nm.

was measured (Fig. 18). It can be seen that Red305 is the most stable dye, as was also concluded from the measurements above. The time dependence of the relative absorbances of the dye maxima reflect the influence of the seasons, which is in line with earlier results [43]. Moreover, it is clear that the matrix material influences the stability as well. Although Red305 in the commercially available polymer Plexit is already rather stable, the stability is even better when distilled PMMA is used as matrix material. In that case the absorbance shows a very small decrease of only 3% after 85 weeks under outdoor conditions, compared to 11-14% when Plexit is used. These results are very promising for long-term stability of the LSC. However, it has to be noted that the final performance of the LSC is determined by the amount of light that reaches the solar cell, and as is depicted in Fig. 14, the EQE of the LSC can decrease, while the absorbance remains unchanged. This has to be checked for the distilled PMMA sample before drawing any conclusions on the stability of the power conversion efficiency.

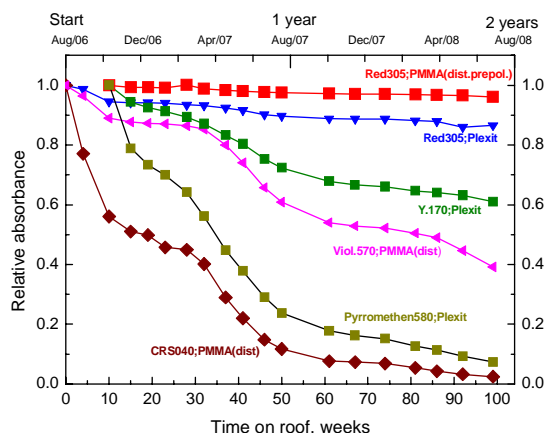


Fig. 18. Relative absorbances in band maxima as a function of time of out-door storage and polymer matrix.

4. Conclusion

We have presented a comprehensive overview of results obtained in the past 5 years on the work performed on luminescent solar concentrators. The renewed interest in the LSCs, since the pioneering work in the 1970s and 1980s, has led to the development of thermodynamic and ray-trace models, which equally well describe the performance of LSCs. Also, new dyes, and more importantly, new quantum dots have been developed and have been included in the polymer concentrators. Stability tests for over 2 years have shown that good candidates exist for use in commercial type LSCs. Still, annual performance of LSCs has to be investigated, as it is expected that better use is made of the diffuse part of solar irradiation compared to conventional solar cells. Finally, cost-optimization studies should prove the economical viability of LSCs.

Acknowledgments

The authors gratefully acknowledge the support from the European Commission through the funding of the project FULLSPECTRUM [10] within the sixth Framework Program (contract number SES6-CT-2003-502620). Michael Debije from the Technical University of Eindhoven, The Netherlands is gratefully acknowledged for supplying information on cholesteric mirrors and test coatings as well for useful discussions. Many thanks are also due Liberato Manna of the NNL-National Nanotechnology Laboratory of CNR-INFN, Lecce, Italy for providing nanorod samples.